Aberrant GluN3A expression increases NMDAR spiking in Huntington's Disease.

Kashif Mahfooz[1], Milos Petrovic[1], Sonia Marco[1], Rebeca Martínez-Turrillas[1], Isabel Pérez-Otaño[1] & John F. Wesseling[1,2]

[1]*CIMA, Dept. Neurociencias, Universidad de Navarra, Pamplona, Spain*

[2]*Corresponding author*

NMDA-type glutamate receptors (NMDARs) are involved in synaptic development and memory formation, but additionally play a computational role in dynamic voltage upstates and action potentials in neuronal dendrites that is analogous to the role of Na^+ channels in axons[1–7]. Here, glutamate binding plays a permissive role and the Mg^{2+} block functions as the voltage gate. So-called NMDAR spikes have not previously been implicated in disease, but NMDAR hyper-function that would promote spiking seems to play a key role that is poorly understood in several major types involving neurodegeneration[8–14]. Here we report a robust increase in NMDAR spiking at early stages in the YAC128 model of Huntington's Disease (HD) that results at the molecular level from aberrant expression of the GluN3A subunit of NMDARs, and at the functional level from stronger synaptic drive. Surprisingly, evidence that HD is caused by enhanced extrasynaptic NMDAR sensitivity to glutamate spilled-over from synaptic clefts was confounded by escape potentials related to NMDAR spikes. Together the new results: introduce NMDAR spikes to medical research by linking aberrant regulation to molecular events that play a causal role in neurodegeneration[15]; question key evidence for

the current concept that NMDAR mis-localization is the pathophysiological trigger, at least in HD[13,16]; show that the stronger synaptic drive in HD[10,17] is caused by GluN3A expression; and establish a more accessible preparation for studying NMDAR spikes.

Medium spiny neurons (MSNs) of the striatum are selectively vulnerable in HD[18]. NMDAR spikes were originally characterized in dendrites of cortical neurons[1], but voltage upstates observed in MSNs *in vivo*[19–21] seems like a related phenomenon because the upstates require NMDAR activation[22,23] and can be induced in *ex vivo* slices by directly applying glutamate to dendrites[23]. Previous attempts to induce NMDAR spikes in MSNs with synaptic input were not successful, possibly because the electrodes for stimulating afferents were placed outside the striatum and did not reproduce the heavy synaptic drive that occurs *in vivo*[20]. However, we were able to induce robust NMDAR spikes in 100 % of current-clamped MSNs in coronal brain slices from 28 - 35 day old mice by placing the stimulating electrode within the striatum (**Fig. 1**).

NMDAR spikes were identified as follows. Axonal spikes were blocked with intracellular Qx314 (5 mM), which blocks voltage-gated Na^+ channels. Weak or moderate afferent stimulation elicited excitatory postsynaptic potentials (EPSPs) with monotonic rising and decay phases that are typical of synaptic responses when they are below threshold for triggering dendritic spikes (blue traces throughout **Fig. 1**). In contrast, stronger stimulation elicited dramatically larger EPSPs that persisted 50 - 150 ms longer and had two distinct rising phases separated by an intermediate decay phase (magenta traces in **Fig. 1**). The timing was similar to NMDAR dependent upstates induced by uncaging glutamate near dendritic branches[23]. The second rising phase was prevented

by NMDAR selective antagonist APV (**Fig. 1a**), confirming involvement of NMDARs. We were not able to back-fire action potentials by injecting current into the cell body (**Extended Data Fig. 1**), confirming previous reports[20,24,25]. Indeed, the second rising phase could not be induced by even tripling the synaptic input in the presence of APV (*e.g.*, **Fig. 1a**, **right panel**), ruling out voltage gated ion channels as the primary mechanism. Finally, the threshold for inducing the second rising phase could be increased by lowering the membrane potential (**Fig. 1b**) or by decreasing EPSP magnitude by partially blocking AMPA-type glutamate receptors with CNQX (not shown), confirming the involvement of regenerative action potentials. We therefore refer to the phenomenon as "NMDAR spikes".

Full-blown NMDAR spikes were clearly distinguishable by eye, but EPSPs that were close to threshold sometimes exhibited intermediate voltage deflections (*e.g.*, the largest amplitude blue traces without APV in **Fig. 1a**). The intermediate deflections might be caused by the failure of spikes in individual dendritic branches to propagate to larger areas of the tree, which is a hallmark of NMDAR spikes and is thought to have important significance for biological computation. Nevertheless, the occurrence made determining threshold parameter values ambiguous in some cases, which could have introduced human biases into the analysis presented next. We therefore developed an automatic algorithm, based on the first derivative dV/dt, for detecting full-blown NMDAR spikes (**Extended Data Fig. 2** and **Supplementary Notes**).

Because altered NMDAR function caused by aberrant expression of GluN3A-containing NMDARs has been linked to HD, we next compared NMDAR spikes in the YAC128 mouse

model of HD and control strains with and without *GluN3A* knocked out[15]. The YAC128 genome contains a transgenic yeast artificial chromosome with the coding sequence for an aggressively pathogenic mutant huntingtin (mHtt) variant. mHtt elevates GluN3A levels by interfering with intracellular protein trafficking, and the aberrant elevation drives progressive morphological and behavioral/motor deficits that are characteristic of HD[15]. We again used 28 - 35 day old mice because the aberrant GluN3A expression and NMDAR dysfunction are already present in YAC128 mice at this stage, whereas compensatory alterations in morphology and connectivity that might have confounded the analysis emerge later[13,17,26]. We found that the threshold stimulating intensity required for inducing NMDAR spikes was almost 3-fold lower in slices from YAC128 mice, but not significantly altered when the aberrant GluN3A expression was prevented in YAC128 mice with *GluN3A* knocked out, or in GluN3A knockouts not expressing mHtt (**Fig. 2a**, **bars**). These results indicate that aberrant GluN3A expression increases NMDAR spiking in the YAC128 model of HD.

Stronger synaptic drive of MSNs has been reported previously in HD models[10,17]. Consistent with this, the slopes of the initial rising phase of EPSPs were steeper in YAC128 MSNs at matched stimulation intensities, including when NMDAR spikes were blocked by APV (not shown). In contrast, no differences were detected in the slopes when the EPSPs generated by the threshold level of stimulation were compared (**Fig. 2a**, **circles**), suggesting that the stronger synaptic drive could account for the lower intensity of stimulation required for inducing NMDAR spikes.

Inspection of raw EPSP traces initially suggested that NMDAR spikes were broader in

YAC128 MSNs (**Fig. 1b**), which might have implied alterations in other mechanisms in addition to stronger synaptic drive. However, the progressive broadening seen for NMDAR spikes for all genotypes as stimulation intensity was increased was expected from the biophysical principles underlying NMDAR spiking[6]. And, no differences were detected when spike widths were plotted against fractional, rather than absolute increases in stimulus intensity above threshold (**Fig. 2b**). This analysis thus suggests that the differences in spike width between YAC128 and other strains was because equivalent stimulation intensities were further above threshold, owing to increased synaptic drive, and likely not because of differences in additional mechanisms.

We next asked whether the stronger synaptic drive of YAC128 MSNs requires GluN3A, as implied by the results in **Fig. 2a**. We confirmed previous findings of excitatory postsynaptic currents (EPSCs) with higher amplitudes over a range of stimulating intensities in voltage clamped YAC128 MSNs compared to WT (**Fig. 3a**)[10,17]. We found further that the higher amplitudes no longer occurred when *GluN3A* was knocked out (**Fig. 3b**), confirming that the stronger synaptic drive of YAC128 MSNs requires the aberrant GluN3A expression[15].

The result could be seen as counterintuitive because NMDARs were blocked by 1mM Mg^{2+} in **Figs. 3a & b**, implying that the heightened EPSC amplitude reflected stronger drive via AMPARs[17], whereas GluN3A is a subunit of NMDARs and is not thought to play a direct role AMPAR function. However, NMDARs in general are coupled to intracellular signaling pathways involved in recruiting/removing AMPARs to/from synapses[27–29], and aberrant GluN3A expression has been reported to drive increases in AMPARs in a different brain region in a model of cocaine abuse[30]. In

any case, analysis of NMDAR/AMPAR ratios after unblocking NMDARs by removing extracellular Mg^{2+} confirmed that the NMDAR component of synaptic transmission was increased along with the AMPAR component (**Fig. 3c**).

Taken together, the results suggest that the increased synaptic drive of YAC128 MSNs caused by aberrant GluN3A expression could account for the increase in NMDAR spiking. However, enhanced NMDAR sensitivity to glutamate that is thought to spill over from synaptic clefts during heavy use has been reported for YAC128 MSNs in addition to the stronger synaptic drive[13]. And, modeling studies indicate that spillover would be especially potent at triggering NMDAR spikes[31]. We therefore tested whether NMDAR spiking could be inhibited with extracellular solution made viscous with 5 % high molecular weight dextran, which prevents extrasynaptic glutamate diffusion in slices[32]. We did not detect any increase in threshold (**Fig. 4a**), however, which was surprising because the electrophysiological evidence for spillover seemed to be robust in previous studies, including our own[13,15].

We therefore re-evaluated the method used previously for detecting spillover. The method was based on the observation that high intensity stimulation evokes long-lasting, outsized NMDAR components of EPSCs. However, we found in a series of experiments that outsized EPSCs are not caused by spillover as supposed, but by NMDAR spikes that continue to occur in voltage clamp mode owing to limitations inherent to the patch-clamp technique; action potentials in voltage clamp mode are termed “escape potentials”. A compelling example experiment is in **Fig. 4b**, which shows that engaging the series resistance (Rs) compensation circuitry of the patch-clamp

amplifier narrows the width of outsized EPSCs to control values. This result is not compatible with glutamate spillover as the cause of outsized EPSCs because series resistance compensation is a cell autonomous manipulation that would not affect glutamate diffusion[33]. Lowering the command potential is also cell-autonomous and produced a similar result (not shown). Additional experiments that rule out spillover in other ways and explain how escape potentials can continue to occur when Mg^{2+} levels are low[34] are described in the **Supplementary Discussion,** and **Extended Data Figs. 4 & 5**; **Extended Data Fig. 3** shows that escape potentials did not confound the NMDAR/AMPAR ratios in **Fig. 3c**, likely because of the extracellular EDTA. Taken together, these results confirm that the decrease in NMDAR spike threshold in the YAC128 model of HD is caused by enhanced synaptic drive and not by enhanced extrasynaptic expression of NMDARs.

NMDAR dysfunction has been hypothesized to drive neurodegeneration in a wide range of diseases[9–14], and indeed neurodegeneration could be prevented in the YAC128 model of HD by preventing developmentally inappropriate re-activation of the GluN3A subunit of NMDARs[15]. Precisely how NMDAR dysfunction causes neurodegeneration is not known, but resolution of this question could greatly expand the range of possible therapeutic targets. One leading hypothesis ascribes toxicity to chronic elevations of intracellular Ca^{2+} [8,9,12,35,36], whereas an opposing hypothesis is that extrasynaptic NMDARs are expressed more abundantly in AD and HD and are inherently toxic because they are selectively coupled to cell death signaling pathways[16]. NMDAR spikes elicit significant Ca^{2+} influx[23], and could thus be the source of toxicity if the chronic Ca^{2+} hypothesis is correct. In contrast, our findings argue against the alternative hypothesis that toxicity is primarily driven by extrasynaptic NMDARs[16], at least in HD, because a key element of the

original evidence is re-interpreted here as arising from NMDAR spikes instead of from increases in the extrasynaptic localization of the NMDARs.

In addition, it is increasingly appreciated that cognitive and neuropsychiatric disturbances occur for many years in a prodromal phase of HD and other neurodegenerative diseases, well before overt signs of neurodegeneration emerge[37,38]. We propose that the disturbances could be caused by increased NMDAR spiking because of the well-established importance of NMDAR spikes in biological computation in other brain regions[1–7].

Finally, it will now be important to determine if NMDAR spiking is also enhanced in AD and other neurodegenerative diseases. It is noteworthy in this context that although the mechanism of memantine action for treating AD is currently thought to be preferential block of extrasynaptic NMDARs, memantine would additionally prevent NMDAR spiking by blocking NMDARs at any dendritic location[39].

References

1. **Schiller, J., Major, G., Koester, H. J. & Schiller, Y. NMDA spikes in basal dendrites of cortical pyramidal neurons.** ***Nature*** **404, 285–9 (2000).**

2. **Major, G., Polsky, A., Denk, W., Schiller, J. & Tank, D. W. Spatiotemporally graded NMDA spike/plateau potentials in basal dendrites of neocortical pyramidal neurons.** ***J.***

Neurophysiol. **99, 2584–601 (2008).**

3. **Polsky, A., Mel, B. & Schiller, J. Encoding and decoding bursts by NMDA spikes in basal dendrites of layer 5 pyramidal neurons. *J. Neurosci.* 29, 11891–903 (2009).**

4. **Ledergerber, D. & Larkum, M. E. Properties of layer 6 pyramidal neuron apical dendrites. *J. Neurosci.* 30, 13031–44 (2010).**

5. **Harnett, M. T., Makara, J. K., Spruston, N., Kath, W. L. & Magee, J. C. Synaptic amplification by dendritic spines enhances input cooperativity. *Nature* 491, 599–602 (2012).**

6. **Major, G., Larkum, M. E. & Schiller, J. Active properties of neocortical pyramidal neuron dendrites. *Annu. Rev. Neurosci.* 36, 1–24 (2013).**

7. **Smith, S. L., Smith, I. T., Branco, T. & Häusser, M. Dendritic spikes enhance stimulus selectivity in cortical neurons in vivo. *Nature* (2013).**

8. **Choi, D. W. Glutamate neurotoxicity and diseases of the nervous system. *Neuron* 1, 623–34 (1988).**

9. **Lipton, S. A. & Rosenberg, P. A. Excitatory amino acids as a final common pathway for neurologic disorders. *N. Engl. J. Med.* 330, 613–22 (1994).**

10. **Levine, M. S. *et al.* Enhanced sensitivity to N-methyl-D-aspartate receptor activation in transgenic and knockin mouse models of Huntington's disease. *J. Neurosci. Res.* 58, 515–32 (1999).**

11. **Bezard, E., Brotchie, J. M. & Gross, C. E. Pathophysiology of levodopa-induced dyskinesia: potential for new therapies.** ***Nat. Rev. Neurosci.*** **2, 577–88 (2001).**

12. **Lipton, S. A. Paradigm shift in neuroprotection by NMDA receptor blockade: memantine and beyond.** ***Nat. Rev. Drug Discov.*** **5, 160–70 (2006).**

13. **Milnerwood, A. J.** ***et al.*** **Early increase in extrasynaptic NMDA receptor signaling and expression contributes to phenotype onset in Huntington's disease mice.** ***Neuron*** **65, 178–90 (2010).**

14. **Costa, A. The Glutamatergic Hypothesis for Down Syndrome: The Potential Use of N-Methyl-D-Aspartate Receptor Antagonists to Enhance Cognition and Decelerate Neurodegeneration.** ***CNS Neurol. Disord. Drug Targets*** **(2013).**

15. **Marco, S.** ***et al.*** **Suppressing aberrant GluN3A expression rescues synaptic and behavioral impairments in Huntington's disease models.** ***Nat. Med.*** **19, 1030–8 (2013).**

16. **Hardingham, G. E. & Bading, H. Synaptic versus extrasynaptic NMDA receptor signalling: implications for neurodegenerative disorders.** ***Nat. Rev. Neurosci.*** **11, 682–96 (2010).**

17. **Joshi, P. R.** ***et al.*** **Age-dependent alterations of corticostriatal activity in the YAC128 mouse model of Huntington disease.** ***J. Neurosci.*** **29, 2414–27 (2009).**

18. **Vonsattel, J. P. & DiFiglia, M. Huntington disease.** ***J. Neuropathol. Exp. Neurol.*** **57, 369–84 (1998).**

19. **Wilson, C. J. & Groves, P. M. Spontaneous firing patterns of identified spiny neurons in the rat neostriatum. *Brain Res.* 220, 67–80 (1981).**

20. **Wilson, C. J. & Kawaguchi, Y. The origins of two-state spontaneous membrane potential fluctuations of neostriatal spiny neurons. *J. Neurosci.* 16, 2397–410 (1996).**

21. **Stern, E. A., Jaeger, D. & Wilson, C. J. Membrane potential synchrony of simultaneously recorded striatal spiny neurons in vivo. *Nature* 394, 475–8 (1998).**

22. **Pomata, P. E., Belluscio, M. a., Riquelme, L. a. & Murer, M. G. NMDA receptor gating of information flow through the striatum in vivo. *J. Neurosci.* 28, 13384–9 (2008).**

23. **Plotkin, J. L., Day, M. & Surmeier, D. J. Synaptically driven state transitions in distal dendrites of striatal spiny neurons. *Nat. Neurosci.* 14, 881–8 (2011).**

24. **Day, M., Wokosin, D., Plotkin, J. L., Tian, X. & Surmeier, D. J. Differential excitability and modulation of striatal medium spiny neuron dendrites. *J. Neurosci.* 28, 11603–14 (2008).**

25. **Carter, A. G. & Sabatini, B. L. State-dependent calcium signaling in dendritic spines of striatal medium spiny neurons. *Neuron* 44, 483–93 (2004).**

26. **Cepeda, C. *et al.* Transient and progressive electrophysiological alterations in the corticostriatal pathway in a mouse model of Huntington's disease. *J. Neurosci.* 23, 961–9 (2003).**

27. **Kessels, H. W., Nabavi, S. & Malinow, R. Metabotropic NMDA receptor function is required for β-amyloid-induced synaptic depression. *Proc. Natl. Acad. Sci. U. S. A.* 110, 4033–8 (2013).**

28. **Roberts, A. C. *et al.* Downregulation of NR3A-containing NMDARs is required for synapse maturation and memory consolidation. *Neuron* 63, 342–56 (2009).**

29. **Shepherd, J. D. & Huganir, R. L. The cell biology of synaptic plasticity: AMPA receptor trafficking. *Annu. Rev. Cell Dev. Biol.* 23, 613–43 (2007).**

30. **Yuan, T. *et al.* Expression of Cocaine-Evoked Synaptic Plasticity by GluN3A-Containing NMDA Receptors. *Neuron* 1–14 (2013).**

31. **Rhodes, P. The properties and implications of NMDA spikes in neocortical pyramidal cells. *J. Neurosci.* 26, 6704–15 (2006).**

32. **Min, M. Y., Rusakov, D. A. & Kullmann, D. M. Activation of AMPA, kainate, and metabotropic receptors at hippocampal mossy fiber synapses: role of glutamate diffusion. *Neuron* 21, 561–70 (1998).**

33. **Sakmann, B. & Neher, E. *Single-Channel Recording* (Springer US, Boston, MA, 1995).**

34. **Antonov, S. M. & Johnson, J. W. Permeant ion regulation of N-methyl-D-aspartate receptor channel block by Mg(2+). *Proc. Natl. Acad. Sci. U. S. A.* 96, 14571–6 (1999).**

35. **Coyle, J. T. & Puttfarcken, P. Oxidative stress, glutamate, and neurodegenerative disorders. *Science* 262, 689–95 (1993).**

36. **Kang, S. *et al.* CaV1.3-selective L-type calcium channel antagonists as potential new therapeutics for Parkinson's disease. *Nat. Commun.* 3, 1146 (2012).**

37. **Selkoe, D. J. Alzheimer's disease is a synaptic failure. *Science* 298, 789–91 (2002).**

38. **Paulsen, J. S. *et al.* Detection of Huntington's disease decades before diagnosis: the Predict-HD study. *J. Neurol. Neurosurg. Psychiatry* 79, 874–80 (2008).**

39. **Chen, H. S. *et al.* Open-channel block of N-methyl-D-aspartate (NMDA) responses by memantine: therapeutic advantage against NMDA receptor-mediated neurotoxicity. *J. Neurosci.* 12, 4427–36 (1992).**

Acknowledgements We thank Aitor Zandueta for technical assistance and Drs. Guy Major, Samuel Wang, Donald Lo, Thomas Aragon, and Montse Arrasate for discussions.

Competing Interests The authors declare that they have no competing financial interests.

Author Contributions KM, MP, and JFW performed experiments. IPO, and JFW designed experiments. SM, RMT, IPO, and JFW designed the mouse breeding strategy. SM and RMT created and maintained the mouse colony, conducted genotyping, and provided mice in a blind fashion. IPO helped edit the manuscript. JFW analyzed the data, and wrote the manuscript.

Correspondence Correspondence and requests for materials should be addressed to J.F.W. (email: johnfwesseling@gmail.com).

Figure 1 NMDAR spikes evoked in striatal MSNs by afferent axon stimulation. Magenta traces were categorized as above threshold by an automatic algorithm described in **Supplementary Figure 2**; blue traces were below threshold. **a.** Examples of recordings used to calculate threshold from individual MSNs. Traces are overlaid responses over a range of stimulation intensities. APV was 50 μM. Graphs in lower panels are the output of the automatic algorithm; green vertical lines mark threshold values. **b.** Hyperpolarization by injecting current into the cell body prevented spiking. **Methods: a & b.** Intracellular solution was (in mM): 120 K-Gluconate, 10 KCl, 8 NaCl, 10 Hepes, 0.5 EGTA, 4 MgATP, 0.3 NaGTP, and 5 Qx314 (pH 7.4); extracellular was 120 NaCl, 26 $NaHC0_3$, 1.25 NaH_2PO_4, 2.5 KCl, 10 Glucose, 2 $CaCl_2$, 1 $MgCl_2$, 0.05 Picrotoxin, 0.02 Glycine, 0.002 Strychnine, bubbled continuously with 95 % O_2/5 % CO_2 gas. **Entire study**: Slices were coronal, 300 μm thick, prepared as described[15] from male mice. The stimulating electrode (Ag/$AgCl_2$) was placed 150 μm away from the cell body[13,15].

Figure 2 GluN3A-dependent increase in NMDAR spiking in YAC128 MSNs. a. Circles: The slopes of the initial rising phase of EPSPs at the threshold stimulation intensity for evoking NMDAR spikes across four genotypes. Bars: Threshold stimulus intensity (n $\geq$ 6; Kolmogorov-Smirnov (KS) test; p < 0.001). **b.** NMDAR spike width was calculated as the time between peak and 50% decay. Solutions were the same as for **Fig. 1**. Experiments were conducted and analyzed blind to genotype; the breeding strategy for homogenizing mouse strain backgrounds was described previously[15].

Figure 3 Stronger synaptic drive in YAC128 caused by GluN3A. a & b. EPSCs were larger in YAC128 MSNs compared to WT, but the difference was abolished when *GluN3A* was knocked out. Stimulus intensity was 60 μA for the example traces (artifacts are blanked). Data are from a subset of MSNs in **Fig. 2** (*i.e.*, extracellular Mg^{2+} was 1 mM); n $\geq$ 5 for each genotype. The command potential was -70 mV. **c.** No decrease in NMDAR/AMPAR ratio in YAC128 MSNs (n = 8 MSNs; 10 traces per MSN were averaged for each condition before analysis). Blue traces were recorded without glutamate receptor blockers; black in 50 μM APV is the AMPAR component; and red is the difference, which is the NMDAR component (traces are averages of all 80 trials). Stimulus intensity was adjusted so that the peak amplitude of EPSCs was 300 pA before adding APV (see **Extended Data Fig. 3**). The extracellular solution contained no added Mg^{2+} and 100 μM EDTA; K^+-channels were blocked by intracellular Cs^+ as described[15]; the command potential was -70 mV.

Figure 4 No evidence for glutamate spillover onto extrasynaptic NMDARs. a. Upper panel is the analysis of a representative experiment. Traces are the EPSPs used to determine threshold for the data points in green, which correspond to ~10 min before dextran application, and ~30 min afterwards. Lower panel: Quantification of all MSNs that survived at least 15 min after dextran application (YAC128; n = 3). Thresholds were normalized by the mean value before applying dextran. Solutions were the same as **Fig. 1** (*i.e.*, 1 mM extracellular Mg^{2+}). **b.** "Strong" stimulation intensity was chosen to be slightly above threshold for evoking outsized EPSCs without Rs compensation. Upper

Panel: Example EPSCs with and without Rs compensation. Lower panel: EPSC width was calculated as the integral divided by the peak; the resulting unit of fC/pA reduced to ms. For statistical analysis: The ratio of EPSC widths with and without Rs compensation was calculated separately for each stimulus intensity, and the ratios for the two intensities were then compared across MSNs (YAC128; n = 5; KS-test $p < 0.001$). At least 3 traces were averaged digitally for each condition for each MSN before further analysis. Solutions were as described[15] (intracellular Cs^{+}; nominally 6 μM extracellular Mg^{2+}). The command potential was -70 mV and Rs compensation was between 50 and 70 % when engaged.

Extended Data Figure 1 Dendritic spikes could not be backfired in MSNs. a. Example traces showing a series of 1 ms current pulses injected in cell bodies of YAC128 MSNs; Na^+ spikes were blocked with Qx314. **b.** Quantification of example in **panel a**. EPSP width was calculated as the integral over 100 ms divided by the peak. The resulting unit mVms/mV reduced to ms. **c.** EPSP width values were normalized by the mean for each MSN before averaging across MSNs (n = 4). Solutions were the same as **Fig. 1** of the main article.

Extended Data Figure 2 Automatic algorithm for detecting NMDAR spikes. The figure compares four strategies for analyzing two examples of wild-type MSNs. All four worked well for automatically detecting NMDAR spikes in the typical example whereas only the algorithm newly developed for the present study worked for the so called worst case example. **a.** Overlaid responses to a range of stimulus intensities. Top panels: after digitally filtering. Middle: first derivatives. Bottom: Positive components of first derivative after the first peak (note the different y-axis scale compared to middle panels). EPSPs detected as above threshold are in magenta. **b.** Four strategies for quantifying the traces all produce non-linear jumps at the threshold stimulus intensity that could, in principle, be used for spike detection. However, the jump compared to scatter is largest in lower right panels where the positive component of the first derivative was integrated over time after the automatically detected first peak in the EPSP response. Symbols: circles are from EPSPs in the absence of APV; crosses are in the presence of APV; squares are from the ratios or differences in the absence and presence of APV.

Extended Data Figure 3 Isolation of the NMDAR component of EPSCs in MSNs. The traces in **panel a** and the data in **panel c** corresponding to "100 % Stim." are also plotted in **Fig. 3c** of the main article. **a**. Blue traces were recorded without glutamate receptor blockers; black in 50 μM APV is the AMPAR component; and red is the difference, which is the NMDAR component; 100 μM EDTA was included throughout. Stimulus intensity corresponding to "100 % Stim." was adjusted so that the peak amplitude of EPSCs was 300 pA before adding APV (duration was 30 μs), whereas "200 % Stim." was double. Data were accepted only if series resistance changed less than 10 %. **b.** Scaled NMDAR components and quantification of time courses. The tail/peak ratio was calculated as the integral over ms 25 - 225 after stimulation divided by the integral over ms 5 - 15, which yields a measure of decay kinetics that does not depend on fitting to a theory. **c.** NMDAR to AMPAR ratios trended higher for YAC128, but the difference was not statistically significant (n = 8 MSNs; KS-test). The similar result at both stimulation intensities rules out involvement of NMDAR escape potentials. **d.** Intensity of stimulation needed to elicit 300 pA EPSCs ($p < 0.002$; KS-test).

Extended Data Figure 4 AMPARs contribute to outsized EPSCs when NMDARs are not blocked. See the **Supplementary Discussion** section for the significance of these data. **a.** No shape change in AMPAR component of EPSCs when isolated from outsized EPSCs by blocking NMDARs. Traces are overlaid recordings of EPSCs without and with 50 μM APV; stimulus artifacts are blanked. "Strong" stimulation was 150 μA for 100 μs. "50 %" was 75 μA and continued to induce outsized EPSCs, although narrower,

because both stimulus intensities were further above threshold than in **Fig. 4b** of the main article; EPSCs were broader for the same reason. Bar graph: Width was calculated by dividing the integral of EPSCs by their peak amplitude (n =3 YAC128 MSNs; KS-test; $p < 0.05$). **b.** AMPARs contribute to outsized EPSCs when NMDARs are not blocked. Traces are overlaid recordings of EPSCs without and with 10 μM CNQX. For these experiments, "Strong" stimulation was ~10 % above the minimum for generating outsized EPSCs. Traces were obtained by averaging the entire data set of at least 3 trials from each MSN. Bar graph: n = 3 YAC128 MSNs; subset of data in **Fig. 4b** of the main article; KS-test $p < 0.05$. Note that series resistance (Rs) compensation continued to narrow dramatically the AMPAR mediated component after strong stimulation (traces obtained after engaging Rs compensation are not shown, but see **Fig. 4b** of the main article).

Extended Data Figure 5 Voltage-dependent blockade of NMDARs in low Mg^{2+}. See the **Supplementary Discussion** section for the significance of these data. y-axis is EPSC peak normalized by the mean of peaks at +20 and +40 mV. x-axis is voltage and was corrected for a liquid junction potential of 14 mV. NMDAR EPSCs were isolated in 10 μM CNQX. Extracellular solution contained only 6 μM Mg^{2+}, and intracellular solution contained Cs^{+} as in **Fig. 4b** of the main article. Series resistance was compensated at between 50 and 70 % (n = 4 MSNs from YAC128 slices).

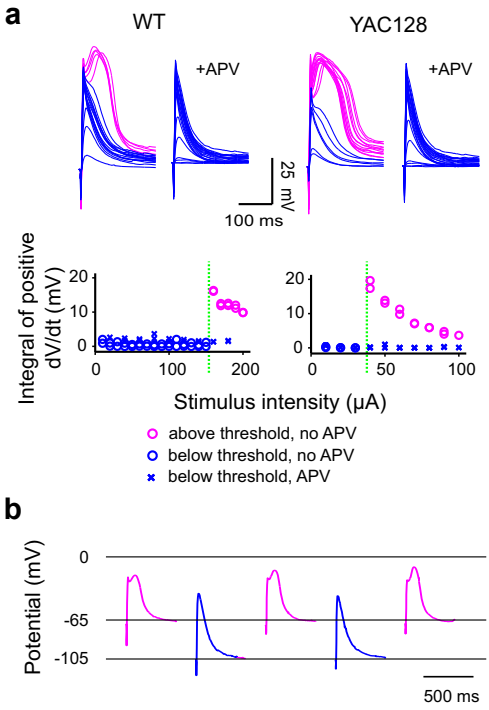
a
WT
YAC128
+APV
+APV
25 mV
100 ms
Integral of positive dV/dt (mV)
20
10
0
0
100
200
20
10
0
0
50
100
Stimulus intensity (μA)
above threshold, no APV
below threshold, no APV
below threshold, APV
b
Potential (mV)
0
-65
-105
500 ms

FIGURE1

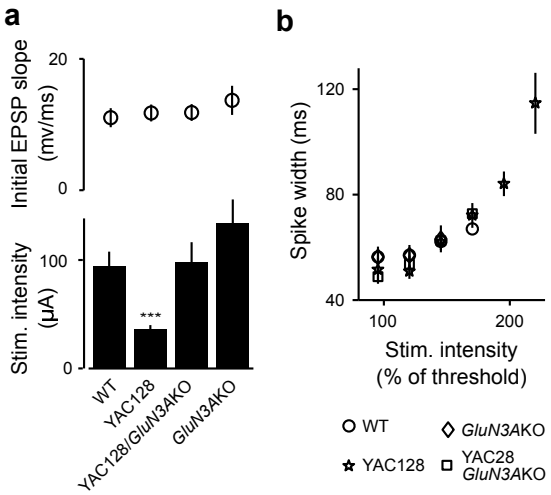
a
Initial EPSP slope (mv/ms)
20
0
Stim. intensity (μA)
100
0
***
WT
YAC128
YAC128/GluN3AKO
GluN3AKO
b
Spike width (ms)
120
80
40
100
200
Stim. intensity (% of threshold)
WT
GluN3AKO
YAC128
YAC28 GluN3AKO

FIGURE 2

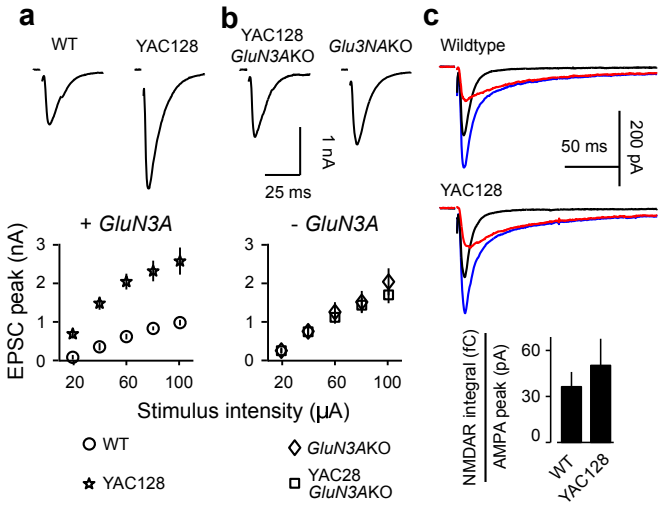
a
WT
YAC128
+ GluN3A
EPSC peak (nA)
Stimulus intensity (μA)
WT
YAC128
b
YAC128
GluN3AKO
Glu3NAKO
1 nA
25 ms
- GluN3A
GluN3AKO
YAC28
GluN3AKO
c
Wildtype
50 ms
200 pA
YAC128
NMDAR integral (fC)
AMPA peak (pA)
WT
YAC128

FIGURE 3

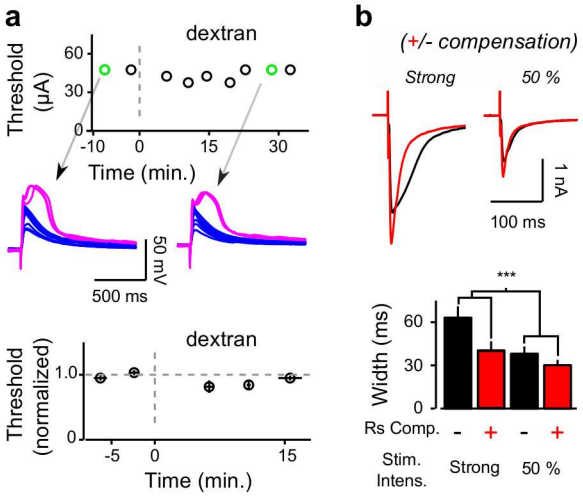
a
dextran
Threshold (µA)
60
30
0
-10
0
15
30
Time (min.)
50 mV
500 ms
dextran
Threshold (normalized)
1.0
0
-5
0
15
Time (min.)
b
(+/- compensation)
Strong
50 %
1 nA
100 ms
***
Width (ms)
60
30
0
Rs Comp.
-
+
-
+
Stim. Intens.
Strong
50 %

FIGURE 4

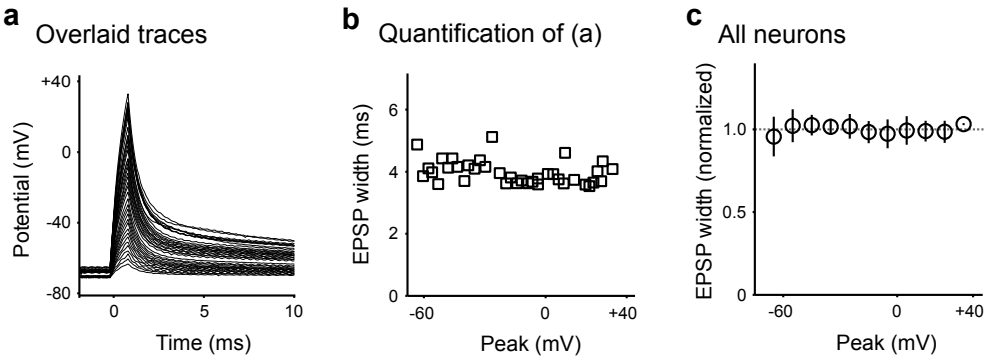

EXTENDED DATA FIGURE 1

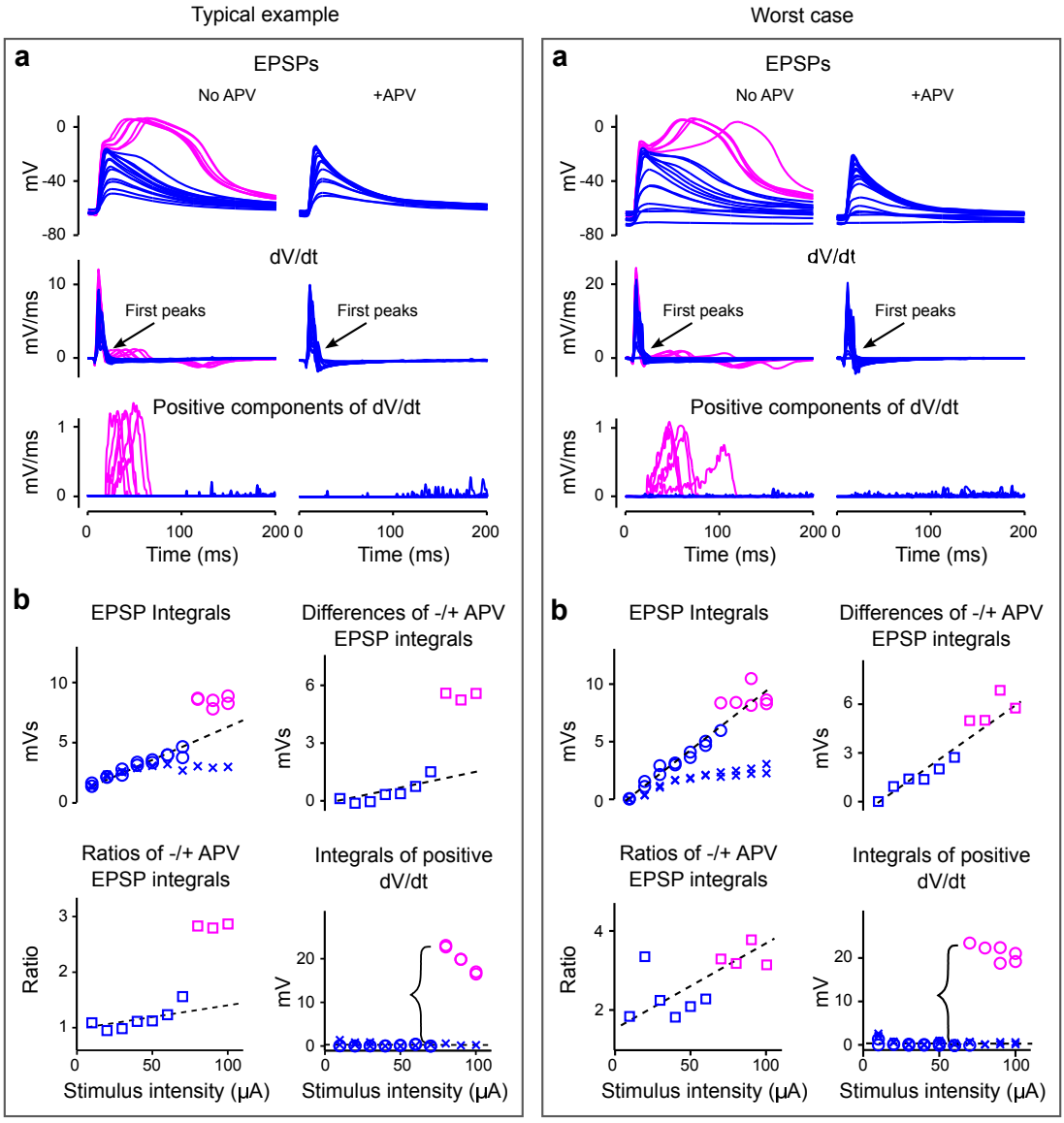

EXTENDED DATA FIGURE 2

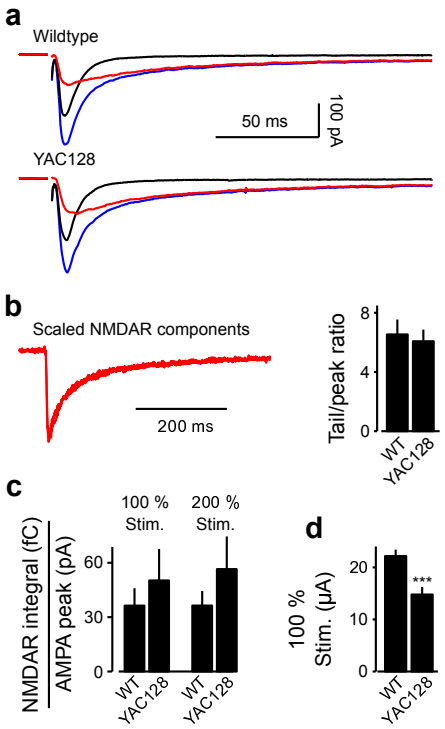

EXTENDED DATA FIGURE 3

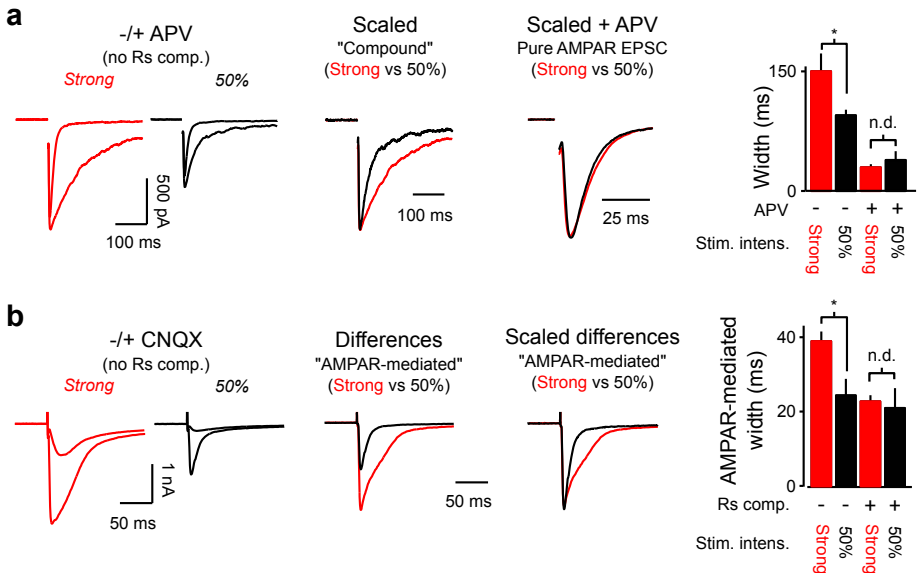

EXTENDED DATA FIGURE 4

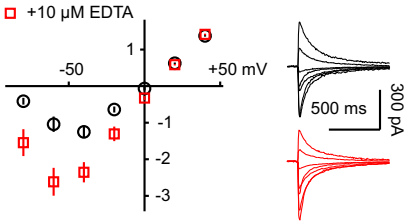

EXTENDED DATA FIGURE 5

Supplementary Information Table of Contents

1 Supplementary Notes for Extended Data Fig. 2

Full-blown NMDAR spikes in MSNs are easily recognized, but some intermediate EPSPs were ambiguous. We therefore developed a simple detection algorithm to avoid biases in determining threshold stimulus intensities.

In previous studies - in other brain regions using a different experimental protocol - discrete jumps in the initially linear relationship between stimulus strength and EPSP amplitude were detected for this purpose[40, 41]. But an identical approach could not be used here because NMDAR spikes were sometimes only induced when the peak of the first rising phase of the EPSP was already close to 0 mV, which is close to the reversal potential for NMDARs and thus close to the maximum. In other words, EPSPs carrying NMDAR spikes were broader, but the peak amplitude was often no higher than the largest subthreshold EPSPs.

The difference compared to the previous studies is likely because afferent input spanned a larger area of the dendritic tree, and likely not because the minimum voltage required for triggering NMDAR spikes in spines of individual dendritic branches was higher[42]. Concerns about non-physiologically intense stimulation were allayed by evidence that activation of ~10 synapses is enough to elicit NMDAR spikes in single dendritic branches[43]; the phenomenon was termed "up-states" in this reference.

The analogous method where the integral of the EPSP was substituted for the peak amplitude (**Extended Data Fig. 2b, upper left panel**) worked well for about half of experiments, but broke down, particularly: (1) when the threshold was high so that the increase in the integral was small compared to trial-to-trial scatter; or (2) when the smallest sub-threshold EPSPs were broader than

larger, but still sub-threshold, EPSPs. The phenomenon of EPSP narrowing did not occur in all MSNs, and the underlying mechanism is not known to us.

More complicated strategies were additionally evaluated, including where the integral of the EPSP recorded without glutamate receptor blockers was divided by the corresponding integral of EPSPs recorded in APV, which blocks NMDARs and thus NMDAR spikes (**Extended Data Fig. 2b, lower left panel**; see also **Extended Data Fig. 2b, upper right panel** where the difference is plotted instead of the ratio). Although better in some cases, these analyses required recordings of the EPSPs in APV, which were not always available. Even when EPSPs in APV were available the analyses continued to break down in some cases (e.g., the "Worst case" example in **Extended Data Fig. 2**), mostly for the same reasons that undermined the measurement based on the integral described above.

We therefore developed a four-step algorithm that was sensitive to the feature of NMDAR spikes that makes them obvious to the human eye, which is the two rising phases separated in time. First, the stimulation artifact was blanked automatically, which was straightforward because it occurred during the same time window in all traces. Second, a point during the first rising phase was detected by finding the maximal value of the first derivative; this worked because the slope of the first rising phase was always steeper than the slope of the second rising phase. Third, the peak of the first rising phase was detected by finding the subsequent point where the first derivative reached zero (**Extended Data Fig. 2a**, **middle panel**). Fourth, subsequent positive first derivative values were summed to calculate an index that was close to zero in the absence of NMDAR spikes, but much greater in their presence (**Extended Data Fig. 2b, lower right panel**). In some cases recording noise complicated the analysis so traces were digitally filtered before calculating the first derivative. The Matlab computer code is listed below.

1.1 Matlab instructions for detecting NMDAR spikes

```
function SpikeIndex = CalculateSpikeIndex(EPSPTrace, BaselineRange, StimArtifactEndPoint)
    Baseline = mean(EPSPTrace(BaselineRange));
    EPSPTrace = EPSPTrace - Baseline;
    EPSPTrace(1:StimArtifactEndPoint) = 0;
    FilteredTrace = filter(GetFilterParameters(),EPSPTrace);
    FirstDerivative = diff(FilteredTrace);
    MaxIndex = GetMaxIndex(FirstDerivative);
    EPSPPeakIndex = FindIndexOfFirstZeroCross(FirstDerivative(MaxIndex:end)) + MaxIndex;
    FirstDerivativeAfterEPSPPeak = FirstDerivative;
    FirstDerivativeAfterEPSPPeak(1:EPSPPeakIndex) = 0;
    FirstDerivativeAfterEPSPPeak(FirstDerivativeAfterEPSPPeak<0) = 0;
    SpikeIndex = sum(FirstDerivativeAfterEPSPPeak);

function index = FindIndexOfFirstZeroCross(array)
```

```
    positions= find(array < 0);
    index = [];
    if not(isempty(positions))
       index = positions(1);
    end;

function index = GetMaxIndex(array)
    mx = max(array);
    positions = find(array==mx);
    index = [];
    if not(isempty(positions))
       index = positions(1);
    end;

function FilterParameters = GetFilterParameters()
    [z,p,k] = cheby1(4,.5,300/(1000*10/2));
    [sos,g] = zp2sos(z,p,k);
    FilterParameters = dfilt.df2tsos(sos,g);
```

2 Supplementary Discussion for Extended Data Figs. 4 & 5

Key evidence for glutamate spillover came from previous electrophysiological experiments where EPSCs elicited by high intensity stimulation were disproportionately outsized and long-lasting in YAC128 MSNs. However, doubts emerged in the present study when a manipulation expected to reduce spillover did not increase the threshold for NMDAR spiking (see **Fig. 4a** of the main article).

EPSCs in the previous experiments were measured in nominally voltage clamped MSNs where spikes would be prevented (under ideal conditions) because a key factor in spiking is membrane depolarization (which would be prevented by an ideal clamp). However, Na^+ spikes, at least, are well known to occur in nominally voltage clamped neurons because of limitations inherent to the patch-clamping technique[44]. We refer to spikes in voltage clamp mode as "escape potentials". Here we show that the outsized EPSCs are caused by NMDAR escape potentials.

2.1 Width of AMPAR-mediated component of EPSCs depends on method for isolation

The first experiment (**Fig. 4b** of the main article) shows that the shapes of outsized EPSCs could be normalized by engaging the series resistance compensation circuitry of the patch-clamp amplifier, whereas smaller EPSCs in the same MSNs evoked by lower intensity stimulation were affected much less. Similar results were obtained by lowering the command potential from -60 to -80 mV (not shown). Both manipulations were most effective when the stimulus intensity was set only a small amount above the minimum needed to elicit outsized EPSCs; outsized EPSCs could still

be generated even with series resistance compensation or at lower command potentials by further increasing the stimulus intensity. Both manipulations would prevent or retard voltage escape to the threshold levels needed for generating NMDAR spikes and the results are therefore in-line with the hypothesis that outsized EPSCs are caused by NMDAR escape potentials. In contrast, the results are not compatible with glutamate spillover as the cause because both manipulations affect MSNs autonomously, and would not impact extracellular diffusion of glutamate.

Furthermore, the pure AMPAR component of EPSCs was not broader when isolated pharmacologically from outsized EPSCs compared to when isolated from smaller EPSCs elicited by lower intensity stimulation[45] (**Extended Data Fig. 4a**). The absence of a change in the shape of the AMPAR component was previously explained by assuming that AMPARs are not activated by extra synaptic glutamate, owing to lower binding affinity. However, we found that the AMPAR mediated component was broader when extrapolated from outsized EPSCs by subtracting the pure NMDAR component isolated pharmacologically with CNQX (**Extended Data Fig. 4b**). This result is not consistent with the spillover explanation for outsized EPSCs because the shape of the AMPAR component should not depend upon the method used for isolating it. In contrast, the result is in line with NMDAR escape potentials because blocking AMPARs would remove most of the depolarizing synaptic drive required to trigger the escape potentials.

Together and separately these results are not consistent with glutamate spillover as the cause of the outsized EPSCs. However, it was not initially clear how NMDAR escape potentials could operate at such low Mg^{2+} levels. That is: the experiments presented here; related experiments published previously[46, 45]; and the ones in **Fig. 4b** of the main article; were all conducted in nominally 6 μM Mg^{2+}, which is too low to block a substantial fraction of NMDARs at negative potentials[47].

2.2 Voltage-dependent NMDAR block in low Mg^{2+}

We therefore measured the current-voltage relationship of synaptic NMDARs and observed voltage dependent blockade, even in nominally 6 μM Mg^{2+} (**Extended Data Fig. 5, black circles**). A similar result has been reported previously for at least one other type of synapse[48]. The result implies the presence of an unknown factor that reversibly blocks NMDARs at hyperpolarized potentials in the absence of Mg^{2+} that could provide the necessary voltage gating for escape potentials. This result thereby removes remaining doubt about the conclusion that outsized EPSCs are caused by NMDAR escape potentials.

The identity of the factor is not known to us. It could be a natural substance contained in brain tissue, or a trace metal contaminant of the reagents. Whatever the identity, however, contaminating Mg^{2+} seems to be unlikely because the voltage-dependence was substantially linearized by only

10 μM EDTA (**Extended Data Fig. 5, red squares**). The factor was therefore less than 10 μM, and consequently must have a higher affinity for blocking NMDARs than Mg^{2+}[47].

3 References

40. Schiller, J., Major, G., Koester, H. J. & Schiller, Y. NMDA spikes in basal dendrites of cortical pyramidal neurons. *Nature* **404**, 285–9 (2000).

41. Major, G., Polsky, A., Denk, W., Schiller, J. & Tank, D. W. Spatiotemporally graded NMDA spike/plateau potentials in basal dendrites of neocortical pyramidal neurons. *J. Neurophysiol.* **99**, 2584–601 (2008).

42. Harnett, M. T., Makara, J. K., Spruston, N., Kath, W. L. & Magee, J. C. Synaptic amplification by dendritic spines enhances input cooperativity. *Nature* **491**, 599–602 (2012).

43. Plotkin, J. L., Day, M. & Surmeier, D. J. Synaptically driven state transitions in distal dendrites of striatal spiny neurons. *Nat. Neurosci.* **14**, 881–8 (2011).

44. Bekkers, J. M. & Stevens, C. F. Excitatory and inhibitory autaptic currents in isolated hippocampal neurons maintained in cell culture. *Proc. Natl. Acad. Sci. U. S. A.* **88**, 7834–8 (1991).

45. Milnerwood, A. J. *et al.* Early increase in extrasynaptic NMDA receptor signaling and expression contributes to phenotype onset in Huntington's disease mice. *Neuron* **65**, 178–90 (2010).

46. Marco, S. *et al.* Suppressing aberrant GluN3A expression rescues synaptic and behavioral impairments in Huntington's disease models. *Nat. Med.* **19**, 1030–8 (2013).

47. Antonov, S. M. & Johnson, J. W. Permeant ion regulation of N-methyl-D-aspartate receptor channel block by Mg(2+). *Proc. Natl. Acad. Sci. U. S. A.* **96**, 14571–6 (1999).

48. Myme, C. I. O., Sugino, K., Turrigiano, G. G. & Nelson, S. B. The NMDA-to-AMPA ratio at synapses onto layer 2/3 pyramidal neurons is conserved across prefrontal and visual cortices. *J. Neurophysiol.* **90**, 771–9 (2003).